

Heterogeneous & Homogeneous & Bio- & Nano-

CHEM **CAT** CHEM

CATALYSIS

Accepted Article

Title: Artificial Photosynthesis of Methanol via Mn:CdS and CdSeTe Quantum Dot co-Sensitized TiO₂ Photocathode in Imine-based Ionic Liquid Aqueous Solution

Authors: Rong Nie, Wenjie Ma, Yapeng Dong, Yanjie Xu, Jinyuan Wang, Jianguo Wang, and Huanwang Jing

This manuscript has been accepted after peer review and appears as an Accepted Article online prior to editing, proofing, and formal publication of the final Version of Record (VoR). This work is currently citable by using the Digital Object Identifier (DOI) given below. The VoR will be published online in Early View as soon as possible and may be different to this Accepted Article as a result of editing. Readers should obtain the VoR from the journal website shown below when it is published to ensure accuracy of information. The authors are responsible for the content of this Accepted Article.

To be cited as: *ChemCatChem* 10.1002/cctc.201800190

Link to VoR: <http://dx.doi.org/10.1002/cctc.201800190>

Artificial Photosynthesis of Methanol via Mn:CdS and CdSeTe Quantum Dot co-Sensitized TiO₂ Photocathode in Imine-based Ionic Liquid Aqueous Solution

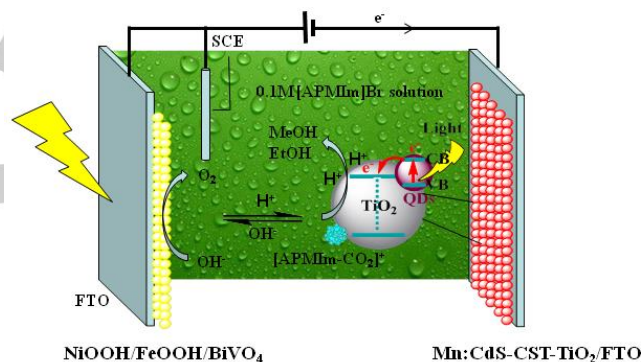
Rong Nie,^{[a],[b]} Wenjie Ma,^[b] Yapeng Dong,^[a] Yanjie Xu,^[a] Jinyuan Wang,^[a] Jianguo Wang^[c] and Huanwang Jing*^{[a],[c]}

Abstract: The artificial photosynthesis (APS) of carbon-based chemicals from CO₂ and water is a promising strategy for solar energy conversion and storage. A new Mn doped CdS and CdSeTe quantum dot co-sensitized TiO₂ photocathode was fabricated and applied to CO₂ reduction in a APS cell with modified BiVO₄ as a counter electrode. The 3D structure of photocathode constructed by Mn:CdS and CdSeTe QDs shown high-efficiency for light harvestings and electrons transfer in this system, resulting methanol in a rate of 90 μM h⁻¹ cm⁻² at -0.9 V vs SCE under 200 mW/cm² irradiation. The methanol could also be produced by a two-electrode system at the same condition. The ¹³CO₂ labeling experiments certified that the carbon-based products are derived from CO₂. On the basis of the experiment results, the mechanism of CO₂ reduction in this new APS cell was proposed as well. In addition, the technique of headspace gas chromatography was used to quantify the products by an external standard method.

Introduction

Nowadays, the abuse of fossil fuels in the world is considered as the main reason for CO₂ emissions, that eventually caused the serious problem in climate change and energy crisis.^[1] Thus, many researchers have devoted to explore new strategies for CO₂ conversion and storage.^[2] The photocatalytic (PC) and photoelectrocatalytic (PEC) reduction of CO₂ have received increasing attention following the pioneer work of Halmann in 1978,^[3] because these methods are clean and environmentally friendly for cyclic utilization of CO₂. The transform of CO₂ can not only decrease the concentration of CO₂ in atmosphere but also provide value-added chemicals.^[4] The PEC reduction of CO₂ in aqueous solution by TiO₂ semiconductor was first reported by Honda in 1979.^[5] Since then, TiO₂-based catalysts have been widely investigated in PEC

reduction of CO₂ due to their low cost, non toxicity, stable chemical property and high resistance to photocorrosion.^[6] However, these catalysts with large band gap ($E_g = 3.0\text{--}3.2\text{ eV}$) still have some drawbacks of narrow absorption in the visible light region.^[6e] In order to improve the photocatalytic efficiency of TiO₂, it is one of the most effective methods to dope a narrow band gap material on the surface of TiO₂. Thus, the generated sensitization structure with cascade band-edge levels can greatly enhance the light-harvesting abilities and promote photoelectron transfer.^[6e, 7]



Scheme 1. Schematic diagram of new APS cell for CO₂ reduction.

Depositing quantum dots (QDs), such as CdS, CdSe, CdTe and CdSeTe have been certified as an efficient strategy for improving the light harvesting of TiO₂ compared with the organic dyes.^[8] These QDs modified semiconductors also have the advantages of long lifetime and high photoelectric conversion efficiency. Recently, some studies shown that doping of transition metal ion into sulfide QDs, such as doping Mn²⁺ into CdS, is a practical method to enhance the electrical and optical properties of QDs, which can increase the efficiency of QDs-sensitized solar cells.^[9]

Inspiring by the above strategies, our group have successfully prepared Mn doped CdS and CdSeTe (CST) QDs co-sensitized TiO₂/FTO photocathodes (named MCCE). For the comparison, TiO₂/FTO, CST-TiO₂/FTO, and CdS-CST-TiO₂/FTO electrodes were also fabricated, and signed as TE, CE and CCE, respectively. In order to set up a new type of APS cell for CO₂ reduction, we choose modified BiVO₄ as photoanode on account of its promising performance in PEC water oxidation.^[10] Meanwhile, a imine-based ionic liquid solution (1-aminopropyl-3-methylimidazoliumbromide, [APMIm]Br ILs) was selected as electrolyte for mimicking the plant environment owing to the properties of negligible volatility, high thermal, chemical stability,

[a] Dr. R. Nie, Mr. Y. Dong, Dr. Y. Xu, Dr. J. Wang, Prof. Dr. H. Jing
State Key Laboratory of Applied Organic Chemistry, College of
Chemistry and Chemical Engineering
Lanzhou University
222 South Tianshui Road, Lanzhou 730000, P. R. China
E-mail: hwjing@lzu.edu.cn

[b] Dr. R. Nie, Mr. W. Ma
Gansu Province Centre for Disease Control and Prevention
335 West Donggang Road, Lanzhou 730000, P. R. China

[c] Prof. Dr. J. Wang, Prof. Dr. H. Jing
State Key Laboratory of Coal Conversion
Institute of Coal Chemistry, Chinese Academy of Sciences
Taiyuan 030001, P. R. China.

Supporting information for this article is given via a link at the end of the document.

wide potential windows and intrinsic conductivity as well as high solubility of CO_2 .^[11] Under charged by an external voltage by an electrochemical workstation or a commercial solar cell, this new designed APS cell can realize efficiently in CO_2 reduction to produce methanol.

Results and Discussion

Structural characteristics of electrodes

The morphologies and microstructures of photocathodes TE and MCCE were characterized by SEM. It can be seen from Fig. 1a that the spherical nanoparticles TiO_2 were firmly coated on the FTO glass surface. After immobilizing Mn: CdS and CST QDs onto TiO_2 nanoparticles, the black quantum dots are dispersed uniformly on the surfaces of TiO_2 with about $0.5\mu\text{m}$ thickness (Fig. 1b and 1c), forming a 3D mesoporous structure. The elements distribution of SEM shows as well this uniformity (Fig. S1). And the EDX spectra confirms the presence of Ti, Cd, Se, Te, Mn, Zn, S, and O elements on the surface of the electrodes (Fig S2). The high resolution TEM image of the electrode MCCE illustrated in Fig. 3d shows clear fringes with lattice spacing of 3.5 \AA , 3.6 \AA and 2.0 \AA , corresponding to the crystal faces of TiO_2 (101), CdSeTe (001) and CdS (110), respectively. The element mapping images (Fig. S3) demonstrate that the all elements are well distributed onto the surfaces of the TiO_2 nanoparticles. The XRD patterns of the photocathodes are shown in Fig. S4. The results illustrate that the prepared electrodes possess similar XRD patterns, exhibiting diffraction peaks of the anatase TiO_2 and SnO_2 , but no diffraction peaks related to QDs, indicating the low content and high dispersion in the surfaces of TiO_2 .^[12] The topography of the electrodes were also observed by atomic force microscopy (AFM) and shown in Fig.S5. The roughness were 28.7 , 17.9 , 16.5 and 15.3 nm for TE, CE, CCE and MCCE, respectively.

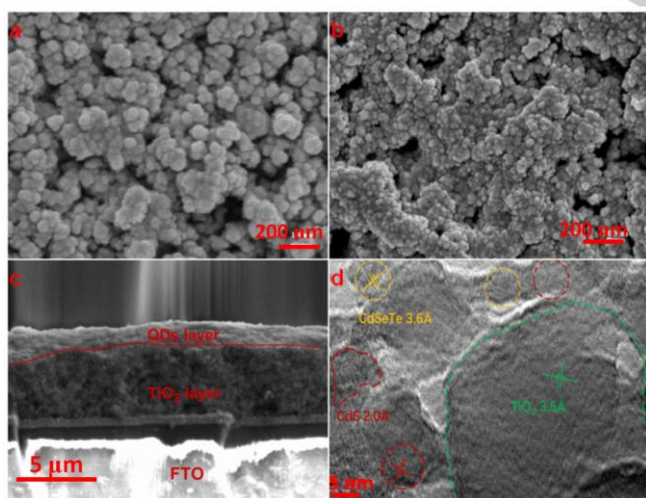


Figure 1. (a) SEM image of bare TiO_2/FTO electrode (TE); (b) SEM image (top view) of MCCE; (c) SEM image (side view) of MCCE; (d) HRTEM image of MCCE.

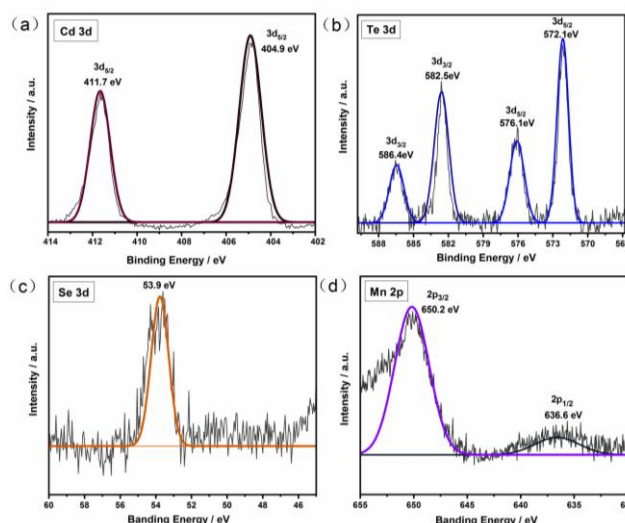


Figure 2. The high-resolution XPS spectra of MCCE: (a) Cd 3d; (b) Te 3d; (c) Se 3d; (d) Mn 2p.

The chemical components and the oxidation states of the CST and Mn: CdS QD co-sensitized FTO/TiO_2 photocathode were characterized by XPS technique. The wide scan XPS spectrum depicted in Fig. S6 revealed the presence of Ti, Cd, Se, Te, Mn, Zn, S, and O characteristic peaks. The high-resolution Cd 3d XPS spectrum (Fig. 2a) has two peaks at 411.7 and 404.9 eV, which belong to Cd $3d_{5/2}$ and Cd $3d_{3/2}$, respectively. The characteristic XPS region spectra of Te $3d_{5/2}$ at 572.1 eV and Te $3d_{3/2}$ at 582.5 eV in Figure 2b reveals the appearance of additional peaks of them. The Te $3d_{5/2}$ peak at 572.1 eV corresponds to Te-Cd bond, and the additional peak at 576.1 eV corresponds to Te-Se bond. As shown in Fig. 2c and 2d, the characteristic peaks of Se 3d are observed at 53.9 eV, the characteristic peaks of Mn 2p located at 650.2 and 636.6 eV belong to Mn $2p_{1/2}$ and $2p_{3/2}$, respectively. All these data are consistent with the standard data laboratory, indicating that CST and Mn: CdS QDs have been successfully decorated onto the surfaces of TiO_2 .

Photoelectrochemical properties of photocathodes

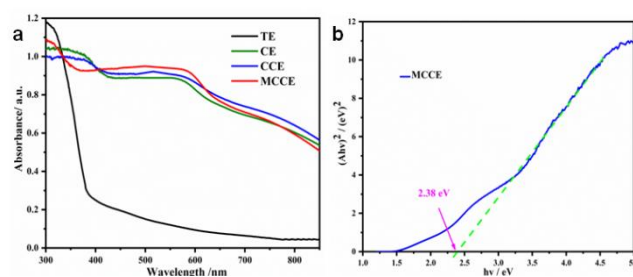


Figure 3. (a) The solid-state UV-vis absorption spectra of photocathodes, (b) the corresponding Tauc plot of MCCE.

The optical absorption properties of the QDs sensitized TiO₂ electrodes were characterized by UV-vis absorption spectra (Fig. 3a). Obviously, the UV-vis absorption bands of CST QDs sensitized TiO₂ electrodes extend to the visible light range (350–850 nm) with very strong absorbance. After subsequent SILAR growth of CdS or Mn:CdS on the CST QDs, the light absorption intensities are further enhanced. It is worth noting that the optical absorption onset of Mn-doped MCCE is broader than that of the non-doped CCE. This extended absorption range could be attributed to a slightly broader size distribution in doped electrode resulting from the incorporation of Mn into the crystal lattice of CdS.^[13] Besides, the band gap of representative MCCE is 2.38 eV (Fig. 3b), which is blue-shifted compare with that of CE and CCE (Fig. S7), indicating that Mn:CdS and CdSeTe QDs co-sensitized materials with a narrow band gap is more beneficial to utilize solar energy for photocatalytic reactions.^[14]

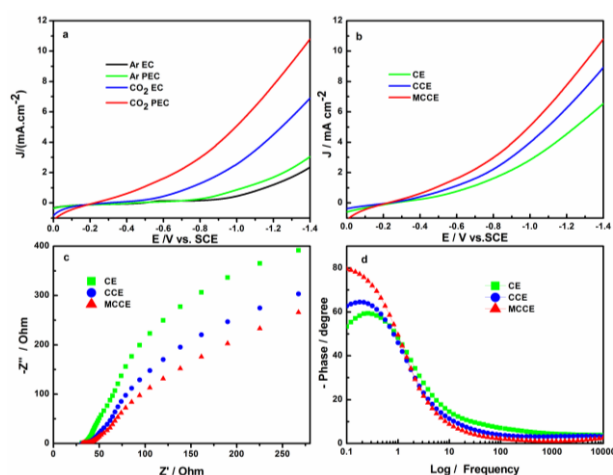


Figure 4. (a) LSV curves of the electrode MCCE in 0.1 M [APMm]Br aqueous solution saturated with Ar or CO₂ under dark or irradiation (200 mW/cm²) with potential; (b) LSV curves of CE, CCE, and MCCE in 0.1 M [APMm]Br aqueous solution saturated with CO₂ under irradiation (200 mW/cm²) with potential; (c) Nyquist plots and (d) Bode plots of the electrodes CE, CCE and MCCE.

The LSV curves for working electrode MCCE presented in Fig. 4a indicate that the current density in the Ar atmosphere is obviously increased from the black line of EC cell to green line of PEC cell in the range of $-0.2 \sim -1.4$ V. When under CO₂ saturation conditions, the photocurrent density has also increased from the blue line of EC cell to the red line of PEC cell resulting from the photoelectrons generated on the electrode surface inject into APS system. In addition, the current density in the CO₂ atmosphere are 5 times than that in the Ar atmosphere. These phenomena imply that the electrode MCCE has excellent photosensitivity in the APS system for CO₂ reduction. Fig. 4b compares the photocurrent densities of the APS cells based on different electrodes (CE, CCE, MCCE). Apparently, the photocurrent densities of CdS or Mn doped CdS/CdSeTe cosensitized electrodes (CCE and MCCE) are much higher than

that of single CST sensitized electrode CE, because the semiconductor heterostructures composing of multiple components bring about a staggered band offset, which is conducive to the absorption of visible light.^[13b] Moreover, when the Mn is doped into the CdS, the photocurrent densities is further increased, which was mainly because the modified Mn:CdS shells not only increased the absorption of visible light but also depressed the electron-hole recombination, leading to the enhancement of photon to current conversion efficiency.^[12, 15] Electrochemical impedance spectroscopy (EIS) is a valid methods for characterizing interface properties of the electrodes. As plotted in Fig. 4c, smaller semicircle represents a lower resistance (R_{ct}) between electrode MCCE and electrolyte. The R_{ct} values of MCCE are much lower than those of other electrodes, leading to more effective separation of the photoelectron-hole pairs and faster interfacial charge transfer.^[16] Beyond that, it can be clearly seen in Bode plots (Fig. 4d) that the electrode MCCE has the lowest characteristic frequency, suggests MCCE can provides a more favorable environment for charge transfer across the interface to PEC reactions.

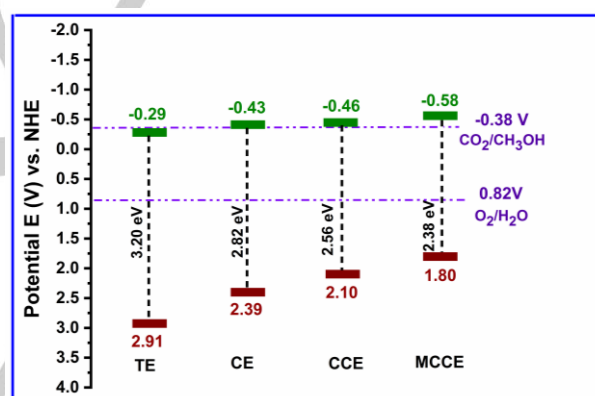


Figure 5. The relative potentials and band gaps of the electrodes TE, CE, CCE and MCCE.^[17]

The positive slopes of Mott-Schottky plots (Fig. S8) indicate that all the prepared electrodes behave as n-type semiconductors. The band position of various sensitized electrodes and the requirements of reduction potential of methanol are illustrated in Fig. 5. The band edges of modified electrodes were moved to negative potentials due to significant quantum confinement effects, indicating that the effective bandgaps become narrow.^[9a] Evidently, the target photocathode MCCE possesses a more negative conduction band position (-0.58 V) than the thermodynamic potential for CO₂ reduction to methanol (-0.38 V). Additionally, its valence band potential loaded at 1.80 V, which is higher than the oxidation potential of O₂/H₂O (0.82 V). These results predict that the photocathode MCCE have excellent photosensitivity in the APS system for CO₂ reduction and water splitting simultaneously.

In addition, the prepared BiVO₄ photoanode was characterized as well by XRD patterns and UV-vis absorption spectra and

illustrated in Fig. S9. The results is well agreement with the reported literature.^[19]

Artificial photosynthetic experiments

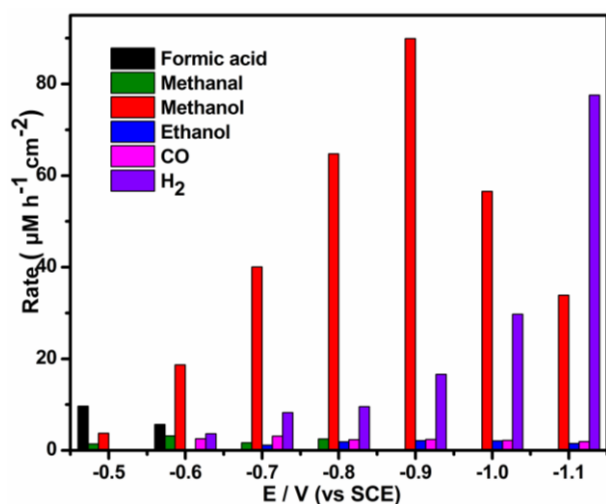


Figure 6. The distribution of products and their formation rates on the photocathode MCCE at various bias potentials in 0.1M [APMIm]Br ILs.

As is well known, the products distribution and the conversion efficiency of CO_2 are highly sensitive to photocathode potential.^[18] So, the APS experiments were firstly carried out using photocathode MCCE at the various bias potentials (from -0.5 V to -1.1 V) in 0.1M [APMIm]Br ILs electrolyte. The formation rates and selectivities of reduction products were depicted in Fig. 6 and Tables S1. It is clear to see that the methanol was the major product accompanying with some ethanol, formic acid and methanal as side products in liquid phase. CO , H_2 and O_2 can be examined in gas phase with low concentrations. The highest formation rate of methanol can approach to $90 \mu\text{M h}^{-1} \text{cm}^{-2}$ at -0.9 V bias potential because more H_2 released at higher potential. Ethanol can be detected when the potential was over to -0.6 V. When the external voltage increased from -0.6 to -1.1 V, the H_2 evolution was elevated from 3.64 to $77.56 \mu\text{M h}^{-1} \text{cm}^{-2}$. All these phenomena reveal that this new prepared photocathode has excellent abilities both in CO_2 reduction and H_2 evolution.

The APS experiments were also carried out using photocathode MCCE in different electrolytes at -0.9 V of external voltage. When 0.1M KHCO_3 was applied as electrolyte, only small amount of methanol ($11.6 \mu\text{M h}^{-1} \text{cm}^{-2}$) was detected (Fig. 7, and Table S2). When the various concentrations of [APMIm]Br ILs was utilized, the rate for the alcohols formation is in the order of $0.1\text{M} > 0.15\text{M} > 0.05\text{M} > 0.2\text{M}$. These phenomena are mainly ascribed to the following reasons:^[19] the high concentration of ionic liquids could enlarge the concentration of CO_2 in electrolyte and is more beneficial to boost the reduction reaction. Whereas, the higher concentration of ionic liquids with larger viscosity might reduces the transportation of protons and hydroxyl ions, which badly suppress the reduction reaction. These results

illuminate that a proper concentration of ionic liquids can accelerate the CO_2 reduction process and benefit the coupling of CO_2 reduction and water splitting to generate hydrocarbon.

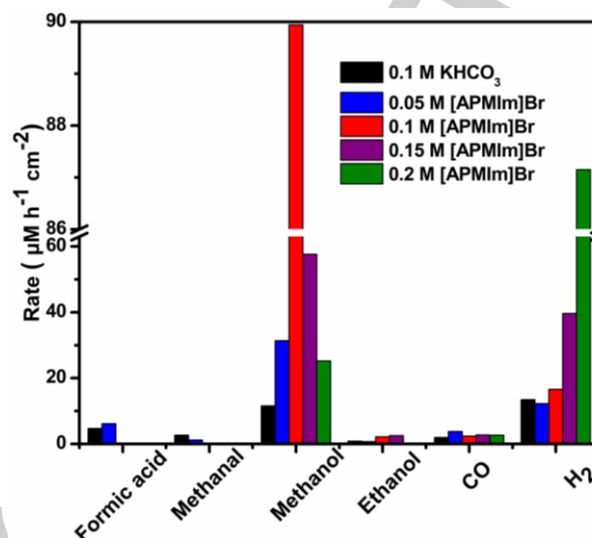


Figure 7. Products formation rates in different electrolytes over MCCE at -0.9 V bias potential (vs. SCE).

The role of different sensitizer were investigated as well. Initially, the experiment was carried out using the single CST QDs sensitized photocathode CE at -0.9 V, only a small quantity of methanol accompanying with much formic acid and methanal were measured (Fig. 8 and Table S3). When CdS and CST QDs co-sensitized photocathode CCE was utilized, the formation rates of methanol increased evidently and a little ethanol was detected. When the target photocathode MCCE was applied to the APS cell, the generated methanol is about 2.5 times higher than that of non-doped photocathode CCE. Meanwhile, the yield of ethanol was increased slightly, but the other side products, such as formic acid and methanal were decreased obviously. This result demonstrates that the target photocathode MCCE possess high selectivity for producing alcohols in the APS cell. The remarkable improvements can be attributed to the synergistic effect of CdS, CdSeTe QDs and TiO_2 substrate, which efficiently promote the electron-hole separation, and give high photoelectron mobility among the semiconductors.^[15] Besides, the doped Mn^{2+} in CdS also obviously depressed the charge recombination, enabled the photogenerated electron-hole pairs to quickly separate into the conduction band of CdS that is more beneficial for reduction reaction.^[20]

The APS experiments using only visible light irradiation ($>400\text{nm}$) were inspected likewise. The formation rate of methanol still kept to $54.6 \mu\text{M cm}^{-2} \text{h}^{-1}$ after 4 h irradiations, which is about 60% of product under full spectra of solar light irradiation. These results present an unprecedented proof-of-concept that the as prepared photocathode MCCE could efficiently reduce the highly stable CO_2 to methanol by harvesting the low-energy visible light photons under very mild reaction conditions. On the other hand,

the stability of the target photocathode MCCE was investigated as well. In five successive experiments, the formation rates of methanol was slight decreased (Fig. S10) and the photocurrent density (J) of the PEC cell seldom decreased during 20 h irradiation (Fig. S11). It revealed that the Mn:CdS and CdSeTe QDs co-sensitized TiO₂ photocathode was quite stable.

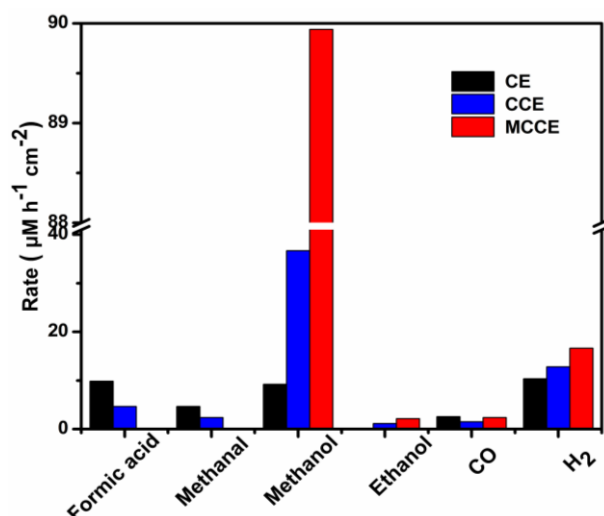


Figure 8. The activities comparison of photocathodes CE, CCE and MCCE in 0.1 M [APMm]Br ILs at -0.9V bias potential (vs. SCE).

In contrast with these APS cells of tri-electrode system, a standard two-electrode APS cell with the photocathode MCCE and BiVO₄ photoanode was built up and investigated. The formation rates of products and light quantum efficiency (QE) at different voltages were illustrated in Fig. 9 and Table S4. The highest QE of this APS cell (Φ_{cell}) is up to 0.58 % at -0.9 V that is higher than 0.4% of plants in nature. When the voltage reached to -1.0 V, the hydrogen yield is sharply increase by electrocatalytic water splitting, while the yield of methanol is decrease obviously.

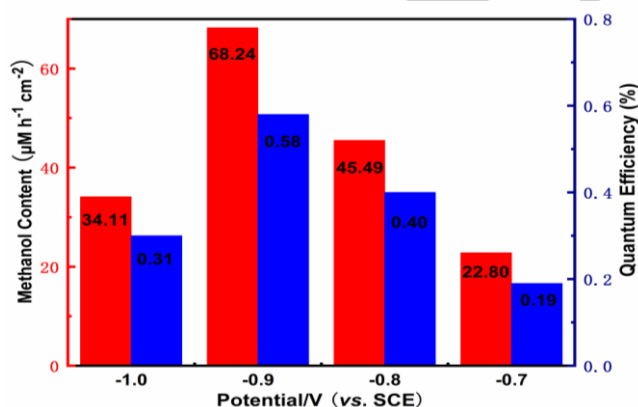


Figure 9. The formation rates and the QE for methanol in the standard two-electrode APS cell under various voltages.

Isotopic labeling experiments of ¹³CO₂ and H₂O¹⁸

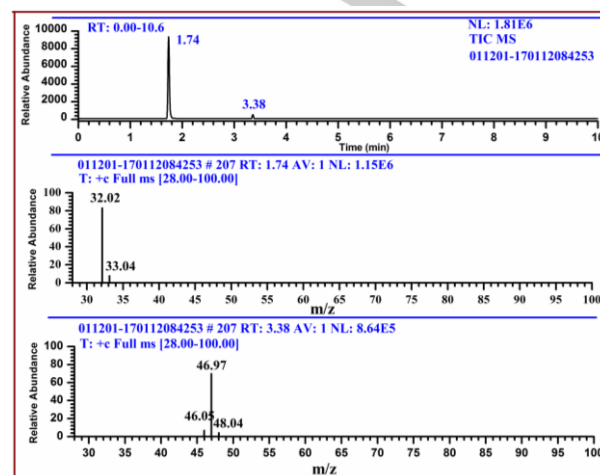


Figure 10. GC-MS analysis for products in the electrolyte of ¹³CO₂ labeling experiment.

To identify the origin of products, ¹³C-labeling isotopic experiments were carefully carried out in the APS cell using the photocathode MCCE. The products in the electrolyte were analyzed by GC-MS (Thermo Fisher, ITQ 900) using an automatic headspace injector. As shown in Fig. 10, the products processing the retention time of 1.74 and 3.83 min related to the m/z value of 32 and 47 can be assigned to ¹³CH₃OH and ¹³CH₃¹³CH₂OH, respectively. This is a very solid evidence to prove that the carbon atoms of alcohols were absolutely stemmed from CO₂. For the purpose of validating the involvement of CO₂ in the reaction, the controlled experiment in high purity Ar gas atmosphere was conducted as well under the same reaction conditions. After 4 hours reaction, no product was detected.

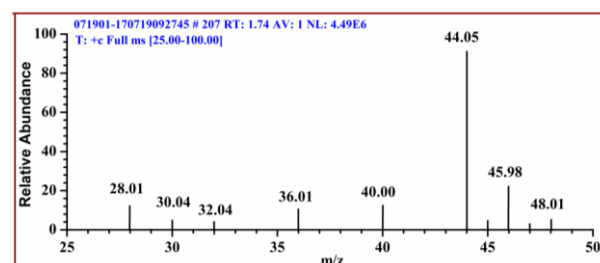


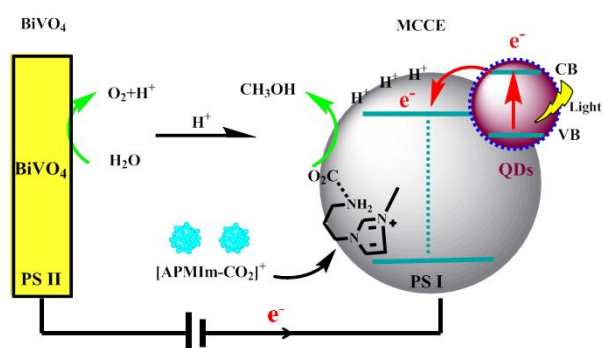
Figure 11. GC-MS analysis for products in gas phase of H₂O¹⁸ labeling experiment.

In addition, the formation rates of gas products are far less than that of methanol in electrolyte, especially for oxygen, which is similar to our previous reports.^[21] In order to prove the speculation that the oxygen might be consumed by the in-situ generated CO, another isotopic labeling reaction of H₂O¹⁸ was

carried out under the similar reaction conditions. Both gas and liquid products were detected by GC–MS. The mass spectrum of products in gas phase exhibits m/z values of 30, 36, 46 and 48 (Fig. 11) that can be assigned to $C^{18}O$ (30), $^{18}O_2$ (36) and $CO^{18}O$ (46), $C^{18}O_2$ (48), respectively. Simultaneously, the mass spectrum of products in the electrolyte demonstrates $CH_3^{18}OH$ ($m/z = 33$) and $CH_3CH_2^{18}OH$ ($m/z = 47$) (Fig. S12). The results are just as our conjecture.

Herein, differing to the reported NMR analysis technique, we adopt a technique, headspace gas chromatography (HS-GC, Agilent 7890A) to quantify the products by an external standard method because the imine-based [APMIm]Br ILs exhibited many peaks in 1H NMR spectrum (Figure S13), which can seriously affect the accuracy of the measurement. The results were also verified using 1H NMR method (Figure S13 and S14). We can see that the result analyzed by HS-GC technique is really better than that analyzed by the 1H NMR technique, which can be seen as well from the good linear relationship of the calibration curves of methanol and ethanol (Figure S15). After analyzing these data, the relative standard deviations (RSD) between the two methods are less than 5%.

Mechanism investigation



Scheme 2. A proposed mechanism for the artificial photosynthesis of chemical fuels.

On the basis of the experiment results, the mechanism is proposed for this APS cell (Scheme 2). It is well known that the electrodes and electrolytes are all of great important in the reduction of CO_2 . In the imine-based [APMIm]Br ILs electrolytes, a complex $[APMIm-CO_2]^+$ can generate quickly through the hydrogen bonding interaction between CO_2 and $[APMIm]^+$ cation^[11a] and then the CO_2 reduction is taken place in the photocathode. Initially, the QDs sensitizer absorbed light energy make the electrons of VB bands jump into the CB bands as active photoelectrons, which can efficiently transfer into the CO_2 reduction reactions. Simultaneously, the protons absorbed on the surface of the photocathode transform to active hydrogen atoms and react with activated CO_2 . In this process, [APMIm]Br ILs can act as co-catalysts during CO_2 reduction by stabilizing catalytic intermediates, which can lower the activation barrier and reduce the overpotential requirement for the reduction of CO_2 to produce the hydrocarbon. Additionally, the water oxidation happened on the photoanode can provide enough H^+

for the CO_2 reduction. Moreover, with the voltage provided by the outer circuit, electrons can fill into the VB band of QDs to complete the recovery.

Conclusions

In this paper, a new APS system composed of Mn:CdS and CdSeTe QDs co-sensitized TiO_2 photocathode and $FeOOH/NiOOH/BiVO_4$ photoanode has been developed aimed to mimicking the natural photosystem I (Calvin cycle) and photosystem II, respectively. We found that the system had a highly efficient catalytic performance for CO_2 reduction to methanol, which was ascribed to the following three aspects: a), the matching energy band gap of the QDs facilitate the light absorption and utilization; b), the material's heterojunction structure lead to the excellent electronic transmission and efficiently depressed the electron-hole recombination, which is beneficial to provide enough electrons for the CO_2 reduction; and c), the application of [APMIm]Br ILs as absorbent and electrolyte can both lower the activation barrier and enhance the conductivity, which is advantageous for accelerating the reduction process. We believe that the combination of functional electrolytes and stable electrodes may provide many opportunities for efficient and economical transformation of CO_2 into valuable chemicals. These findings would be a new perspective artificial photosynthesis system for efficient CO_2 reduction in the near future.

Experimental Section

Preparation of the quantum dots sensitized TiO_2 photocathodes

The fabrication process of electrode TE and CST QDs are listed in the supporting information. Two electrodes TE were immersed into fresh prepared CST QDs solution (10 mL) for 12 h at room temperature. The QDs are tightly anchored onto the surface of TiO_2 nanoparticles by the carboxylic acid groups of 3-mercaptopropionic acid (MPA) via the self-assembly method.^[22] After drying in vacuum oven for 1 h at 70 °C, the electrode CE were successfully obtained and stored in the dark for use.

The desired electrode MCCE was obtained by successive ionic layer adsorption and reaction (SILAR) strategy.^[23] Briefly, a methanol solution (A) containing 0.1 M cadmium acetate and 0.08 M manganese acetate and a water/methanol ($v/v=1:1$) solution (B) containing 0.1 M Na_2S were firstly prepared. The above prepared electrodes CE were dipped alternately into the solution A and B for 1 min and repeated six times. After each step, the electrodes were rinsed with DI water. Lastly, the electrodes were coated with 4 cycles of ZnS by alternately immersion into 0.1 M zinc acetate and 0.1 M Na_2S aqueous solutions for 1 min to stabilize the QDs and reduce the charge recombination of electrons at the TiO_2 /electrolyte interfaces.^[12, 24] The electrode CCE was prepared using the same procedures without manganese acetate.

Photoelectrocatalytic experiments

The photoelectrochemical measurements were carried out on an electrochemical workstation (CHI 660E, Shanghai, China) using a

standard three-electrode system in a sealed quartz APS cell (Scheme 1). The as prepared electrodes (TE, CE, CCE, MCCE) and modified BiVO₄ electrode were served as photocathode and counter electrode (both with an area of 1.4 cm²), respectively. A saturated calomel electrode (SCE) was used as reference electrode. The electrolyte was CO₂ or Ar saturated 0.1 M [APMIm]Br ILs. A 300 W Xe lamp (XD 350, Perfect Light, China) was served as simulated sun light source. The linear sweep voltammetry (LSV) was measured in 0.1 mol L⁻¹ [APMIm]Br ILs swept from 0.0 V to -1.4 V with a scan rate of 50 mV s⁻¹. The electrochemical impedance spectroscopy (EIS) was measured at the open circuit potential both in dark and under irradiation of simulated solar light. The frequency range was from 100000 Hz to 0.1 Hz with an acquisition of 10 points per decade and an amplitude of -5 mV.

Artificial photosynthesis experiment

The artificial photosynthetic experiments was performed in [APMIm]Br ILs (0.05–0.2M, 85 mL) or 0.1M KHCO₃ (PH=6.8, 85mL) under simulated sunlight irradiation and appropriate external potential. The prepared photocathode (CE, CCE, MCCE), BiVO₄ and SCE were served as the working, counter and reference electrode, respectively. Prior to measurements, the electrolyte was bubbled with pure CO₂ (99.9%) or ¹³CO₂ (99.9%) for 30 min to saturate the solution. A 300 W Xe lamp (XD 350, Perfect Light, China) was served as simulated sun light. The products were quantified using headspace gas chromatography (HS-GC, Agilent 7890A) by an external standard method.

Acknowledgements

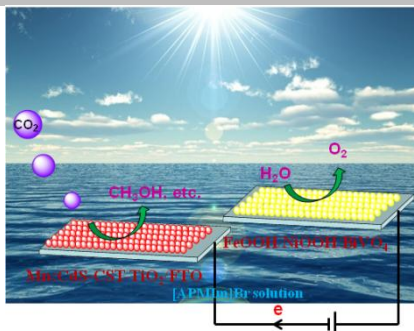
This work was funded by the National Natural Science Foundation of China (NSFC 21173106), the Foundation of State Key Laboratory of Coal Conversion (Grant No. J17-18-913-2), and Natural Science Foundation of Gansu Province (17JR5RA212), College Research Foundation of Gansu (2016B-053).

Keywords: Artificial photosynthesis • Carbon dioxide reduction • Quantum dot • Titanium dioxide • Ionic liquids

- [1] a) R. K. de Richter, T. Ming, S. Caillol, *Renew. Sustain. Energy Rev.* **2013**, *19*, 82-106; b) A. Zecca, L. Chiaia, *Energy Policy* **2010**, *38*, 1-3; c) M. Tahir, N. S. Amin, *Renew. Sustain. Energy Rev.* **2013**, *25*, 560-579.
- [2] a) Z. Zhu, Y. Han, C. Chen, Z. Ding, J. Long, Y. Hou, *ChemCatChem* 10.1002/cctc.201701573; b) U. Rodemerck, M. Holeña, E. Wagner, Q. Smejkal, A. Barkschat, M. Baerns, *ChemCatChem* **2013**, *5*, 1948-1955; c) K. Sekizawa, K. Maeda, K. Domen, K. Koike, O. Ishitani, *J. Am. Chem. Soc.* **2013**, *135*, 4596-4599; d) X. Jiang, F. Gou, F. Chen, H. Jing, *Green Chem.* **2016**, *18*, 3567-3576; e) M. H. Beyzavi, R. C. Klet, S. Tussupbayev, J. Borycz, N. A. Vermeulen, C. J. Cramer, J. F. Stoddart, J. T. Hupp, O. K. Farha, *J. Am. Chem. Soc.* **2014**, *136*, 15861-15864; f) P. Li, H. Wang, J. Xu, H. Jing, J. Zhang, H. Han, F. Lu, *Nanoscale* **2013**, *5*, 11748-11754; g) F. Stedt, I. Sharafutdinov, F. Abild-Pedersen, C. F. Elkjaer, J. S. Hummelshoj, S. Dahl, I. Chorkendorff, J. K. Nørskov, *Nat. Chem.* **2014**, *6*, 320-324; h) S. Zhang, P. Kang, S. Ubnoske, M. K. Brennaman, N. Song, R. L. House, J. T. Glass, T. J. Meyer, *J. Am. Chem. Soc.* **2014**, *136*, 7845-7848; i) Y. Na, P. Lincoln, J. R. Johansson, B. Nordén, *ChemCatChem* **2012**, *4*, 1746-1750.
- [3] M. Halmann, *Nature* **1978**, *275*, 115-116.
- [4] a) B. Kumar, M. Lorente, J. Froehlich, T. Dang, A. Sathum, C. P. Kubiak, *Annu. Rev. Phys. Chem.* **2012**, *63*, 541-569; b) J. L. White, M. F. Baruch, J. E. Pander lii, Y. Hu, I. C. Fortmeyer, J. E. Park, T. Zhang, K. Liao, J. Gu, Y. Yan, T. W. Shaw, E. Abelev, A. B. Bocarsly, *Chem. Rev.* **2015**, *115*, 12888-12935; c) S. Neatu, J. A. Macia-Agullo, P. Concepcion, H. Garcia, *J. Am. Chem. Soc.* **2014**, *136*, 15969-15976; d) C. Ding, A. Li, S.-M. Lu, H. Zhang, C. Li, *ACS Catal.* **2016**, *6*, 6438-6443.
- [5] T. Inoue, A. Fujishima, S. Konishi, K. Honda, *Nature* **1979**, *277*, 637-638.
- [6] a) M. R. Hasan, S. B. Abd Hamid, W. J. Basirun, S. H. Meriam Suhaimy, A. N. Che Mat, *RSC Adv.* **2015**, *5*, 77803-77813; b) O. Ola, M. M. Maroto-Valer, *J. Photochem. Photobio. C: Photochem. Rev.* **2015**, *24*, 16-42; c) J. Yu, J. Low, W. Xiao, P. Zhou, M. Jaroniec, *J. Am. Chem. Soc.* **2014**, *136*, 8839-8842; d) X. Chang, T. Wang, P. Zhang, Y. Wei, J. Zhao, J. Gong, *Angew. Chem. Int. Ed.* **2016**, *55*, 8840-8845; e) Y. Ma, X. Wang, Y. Jia, X. Chen, H. Han, C. Li, *Chem. Rev.* **2014**, *114*, 9987-10043.
- [7] a) P. Li, J. Zhang, H. Wang, H. Jing, J. Xu, X. Sui, H. Hu, H. Yin, *Catal. Sci. Technol.* **2014**, *4*, 1070-1077; b) H. Tada, T. Mitsui, T. Kiyonaga, T. Akita, K. Tanaka, *Nat. Mater.* **2006**, *5*, 782-786; c) T. Di, B. Zhu, B. Chen, J. Yu, J. Xu, *J. Catal.* **2017**, *352*, 532-541.
- [8] a) S. Gu, J. K. Cooper, C. Corrado, B. Vollbrecht, F. Bridges, J. Guo, J. Z. Zhang, *J. Phys. Chem. C* **2011**, *115*, 20864-20875; b) A. Sahasrabudhe, S. Bhattacharyya, *Chem. Mater.* **2015**, *27*, 4848-4859; c) S. Jin, M. Tagliazucchi, H.-J. Son, R. D. Harris, K. O. Aruda, D. J. Weinberg, A. B. Nepomnyashchii, O. K. Farha, J. T. Hupp, E. A. Weiss, *J. Phys. Chem. C* **2015**, *119*, 5195-5202.
- [9] a) J. Tian, L. Lv, C. Fei, Y. Wang, X. Liu, G. Cao, *J. Mater. Chem. A* **2014**, *2*, 19653-19659; b) C. Liu, H. Tang, J. Li, W. Li, Y. Yang, Y. Li, Q. Chen, *RSC Adv.* **2015**, *5*, 35506-35512; c) H.-J. Kim, H.-D. Lee, C. S. S. Pavan Kumar, S. S. Rao, S.-H. Chung, D. Punnoose, *New J. Chem.* **2015**, *39*, 4805-4813.
- [10] T. W. Kim, K. S. Choi, *Science* **2014**, *343*, 990-994.
- [11] a) W. Lu, B. Jia, B. Cui, Y. Zhang, K. Yao, Y. Zhao, J. Wang, *Angew. Chem. Int. Ed.* **2017**, *56*, 11851-11854; b) N. Roy, Y. Shibano, C. Terashima, K.-i. Katsumata, K. Nakata, T. Kondo, M. Yuasa, A. Fujishima, *ChemElectroChem* **2016**, *3*, 1044-1047.
- [12] P. K. Santra, P. V. Kamat, *J. Am. Chem. Soc.* **2012**, *134*, 2508-2511.
- [13] a) M. Azad Malik, P. O'Brien, N. Revaprasadu, *J. Mater. Chem.* **2001**, *11*, 2382-2386; b) L. Yu, Z. Li, Y. Liu, F. Cheng, S. Sun, *Appl. Surf. Sci.* **2014**, *309*, 255-262.
- [14] J. Wang, Y. Li, Q. Shen, T. Izuishi, Z. Pan, K. Zhao, X. Zhong, *J. Mater. Chem. A* **2016**, *4*, 877-886.
- [15] C. V. Gopi, M. Venkata-Haritha, S. K. Kim, H. J. Kim, *Nanoscale* **2015**, *7*, 12552-12563.
- [16] M. Asadi, K. Kim, C. Liu, A. V. Addepalli, P. Abbasi, P. Yasaei, P. Phillips, A. Behranginia, J. Cerrato, R. Haasch, P. Zapol, B. Kumar, R. F. Klie, J. Abiade, L. A. Curtiss, A. Salehi-Khojin, *Science* **2016**, *353*, 467-470.
- [17] Y. Zheng, W. Zhang, Y. Li, J. Chen, B. Yu, J. Wang, L. Zhang, J. Zhang, *Nano. Energy* **2017**, *40*, 512-539.
- [18] R. J. Lim, M. Xie, M. A. Sk, J.-M. Lee, A. Fisher, X. Wang, K. H. Lim, *Catal. Today* **2014**, *233*, 169-180.
- [19] S. Wang, X. Wang, *Angew. Chem. Int. Ed.* **2016**, *55*, 2308-2320.
- [20] H. Zhu, T. Lian, *Energy Environ. Sci.* **2012**, *5*, 9406.
- [21] L. Wang, Y. Jia, R. Nie, Y. Zhang, F. Chen, Z. Zhu, J. Wang, H. Jing, *J. Catal.* **2017**, *349*, 1-7.
- [22] H. Zhang, K. Cheng, Y. M. Hou, Z. Fang, Z. X. Pan, W. J. Wu, J. L. Hua, X. H. Zhong, *Chem. Commun.* **2012**, *48*, 11235-11237.
- [23] J. Luo, H. Wei, Q. Huang, X. Hu, H. Zhao, R. Yu, D. Li, Y. Luo, Q. Meng, *Chem. Commun.* **2013**, *49*, 3881-3883.
- [24] B. C. Fitzmorris, Y. C. Pu, J. K. Cooper, Y. F. Lin, Y. J. Hsu, Y. Li, J. Z. Zhang, *ACS Appl. Mater. Interfaces* **2013**, *5*, 2893-2900.

FULL PAPER

A new Mn doped CdS QDs and CdSeTe QDs co-sensitized TiO₂/FTO electrode with a narrow band gap of 2.38eV is applied for reduction of CO₂ in [APMIm]Br ILs aqueous solution. The PEC cell has high selectivity for producing methanol, with the maximum yield of 90 μM h⁻¹ cm⁻² and the light quantum efficiency of 0.58 %.



Rong Nie, Wenjie Ma, Yapeng Dong,
Yanjie Xu, Jinyuan Wang, Jianguo
Wang, Huanwang Jing*

Page No. – Page No.

**Artificial Photosynthesis of
Methanol via Mn:CdS and CdSeTe
Quantum Dot co-Sensitized TiO₂
Photocathode in Imine-based Ionic
Liquid Aqueous Solution**